Piezoelectric resonance and sound attenuation in the Rochelle salt $NaKC_4H_4O_6 \cdot 4H_2O$

A. P. Moina and R. R. Levitskii
Institute for Condensed Matter Physics, 1 Svientsitskii Street, 79011 Lviv, Ukraine

I. R. Zachek
Lviv Polytechnic National University, 12 Bandery Street, 79013 Lviv, Ukraine
(Received 23 August 2004; published 25 April 2005)

Within the framework of the two-sublattice Mitsui model, taking into account the piezoelectric interaction with the shear strain ε_4, a dynamic dielectric response of Rochelle salt is considered. Experimentally observed phenomena of crystal clamping by high-frequency electric field, piezoelectric resonance, and microwave dispersion are described. Ultrasound velocity and attenuation are calculated, and peculiarities of their temperature dependence at the Curie points are described. Existence of a cutoff frequency in the frequency dependence of attenuation is shown.

DOI: 10.1103/PhysRevB.71.134108 PACS number(s): 77.22.Gm, 77.65.Fs, 77.65.Dq

I. INTRODUCTION

Crystals of Rochelle salt have been attracting the interest of physicists due to their practical applications and, from a fundamental point of view, due to the curious character of their ferroelectric behavior. In contrast to most of the known ferroelectrics, in Rochelle salt the ferroelectric phase exists only in a narrow temperature interval between two second-order phase transitions at 255 and 297 K. Spontaneous polarization is directed along the *a* axis and accompanied by the spontaneous shear strain ε_4. The ferroelectric phase is monoclinic (C_2^2); both paraelectric phases are orthorhombic (D_2^3). Thus Rochelle salt crystals are noncentrosymmetric and piezoelectric in all phases, which essentially affects their dielectric response.

In the frequency dependence of the dielectric permittivity of Rochelle salt, the three following dispersion regions are observed (see, e.g., Ref. 1): (i) domain-related dispersion below 1kHz, present only in the ferroelectric phase,[2,3] (ii) microwave relaxational dispersion, and (iii) piezoelectric resonance in the 10^4-10^7 Hz region, depending on sample dimensions and temperature. Below the resonances the dielectric permittivity of a free crystal is measured, whereas above the resonances the crystal is effectively clamped. A concise explanation of the clamping effect and the resonances is given by the following formula, obtained by Mueller[4] in 1940 for the 1 cm long 45° *X* cuts of Rochelle salt:

$$\chi = \chi_{\text{free}} + \left(1 - \frac{2V}{\omega}\tan\frac{\omega}{2V}\right) d_{12}'^2 s_{22}',$$

where χ_{free} is the free-crystal permittivity, V is the sound velocity, and d_{12}', s_{22}' are the corresponding piezomodule and compliance. Applicability of this formula, however, is limited to the MHz region, since it does not reproduce the microwave dynamics of the permittivity.

The behavior of Rochelle salt is usually described within a two-sublattice Ising model with an asymmetric double-well potential (Mitsui model[5]). Usually it suffices to use the mean-field approximation. Dynamic dielectric response is approached within stochastic Glauber dynamics[6,7] or the Bloch equations method.[8,9]

The conventional Mitsui model does not take into account the piezoelectric coupling with shear strain ε_4. This leads to qualitatively incorrect results yielded by the model for the temperature behavior of microwave relaxation times and dynamic permittivity near the Curie points.[7,10] The origin of such a discrepancy—a fundamental drawback of the conventional model—is that the model does not distinguish free and clamped crystals and is not able to reproduce the effect of crystal clamping by high-frequency electric field (or mechanical stress).

A recently proposed modification of the Mitsui model[11] takes into account the piezoelectric effects. It allows one to calculate, depending on what is necessary (observed in experiment), susceptibilities of either the free or clamped crystal. Thus, setting the clamped crystal regime, we were able to obtain a correct temperature behavior of the microwave dielectric response of Rochelle salt, which was in both qualitative and quantitative agreement with experiment (e.g., Ref. 12) also near the Curie points.

So far the model consideration of dielectric response in Rochelle salt has been restricted to the static limit and to the microwave region. Attempts to explore the piezoelectric resonance phenomenon within a model that does not take into account the piezoelectric coupling are pointless. It seems thus natural to extend the model with piezoelectric coupling[11] onto the entire frequency range from the static limit (in the ferroelectric phase from about 1 kHz) to THz frequencies, including as well the piezoelectric resonance region. For a coupled dynamics of the shear strain ε_4–pseudospin system, the standard methods of description of the lattice strain dynamics[13] based on Newtonian equations of motion will be combined with the Glauber approach to pseudospin dynamics. We shall calculate dynamic dielectric, piezoelectric, and elastic characteristics of Rochelle salt. Evolution of the dielectric permittivity from the static free crystal value via the piezoelectric resonances to the clamped crystal value and to the microwave relaxation will be described. Within the same approach we shall derive expressions for ultrasound velocity and attenuation (for a certain

geometry of sound propagation) and explore their temperature and frequency behavior.

Experimentally sound attenuation in Rochelle salt has been studied since the 1940's[14–17]. In accordance with the Landau and Khalatnikov prediction,[18] an anomalous increase of attenuation associated with the shear strain ε_4 was revealed near the Curie points. So far the theoretical description of this phenomenon has been restricted to that proposed by the Landau approach based on expansions of thermodynamic potential in the order parameter.[15,19] In the present paper the model calculations of attenuation will be performed.

II. THERMODYNAMICS OF THE SYSTEM

Let us present here the main results for the equilibrium thermodynamics of Rochelle salt obtained within the modified Mitsui model.[11] Calculations are performed with the Hamiltonian

$$\hat{H} = NU_{\text{seed}} - \frac{1}{2}\sum_{qq'}\sum_{ff'=1}^{2} R_{qq'}(ff')\frac{\sigma_{qf}}{2}\frac{\sigma_{q'f'}}{2} - \Delta\sum_{q}\left(\frac{\sigma_{q1}}{2} - \frac{\sigma_{q2}}{2}\right) - (\mu_1 E_1 - 2\psi_4\varepsilon_4)\sum_{q}\sum_{f=1}^{2}\frac{\sigma_{qf}}{2}. \tag{2.1}$$

Here

$$U_{\text{seed}} = \frac{v}{2}c_{44}^{E0}\varepsilon_4^2 - ve_{14}^0\varepsilon_4 E_1 - \frac{v}{2}\chi_{11}^{\varepsilon 0}E_1^2$$

is a "seed" energy of the crystal lattice which forms the asymmetric double-well potential for the pseudospins. $R_{qq'}(11)=R_{qq'}(22)=J_{qq'}$ and $R_{qq'}(12)=R_{qq'}(21)=K_{qq'}$ are constants of interaction between pseudospins belonging to the same and to different sublattices, respectively. The parameter Δ describes the asymmetry of the double-well potential; μ_1 is the effective dipole moment. The last term is the internal field created by the piezoelectric coupling with the shear strain ε_4.

Introducing the parameters of ferroelectric and antiferroelectric ordering

$$\xi = \frac{1}{2}(\langle\sigma_{q1}\rangle + \langle\sigma_{q2}\rangle), \quad \sigma = \frac{1}{2}(\langle\sigma_{q1}\rangle - \langle\sigma_{q2}\rangle),$$

within the mean-field approximation, we obtain the thermodynamic potential of the system[11]

$$\frac{g_{1E}}{N} = U_{\text{seed}} + \frac{J+K}{4}\xi^2 + \frac{J-K}{4}\sigma^2 - \frac{2\ln 2}{\beta} - \frac{1}{\beta}\ln\cosh\frac{\gamma+\delta}{2}\cosh\frac{\gamma-\delta}{2} - v\sigma_4\varepsilon_4,$$

where

$$\gamma = \beta\left(\frac{J+K}{2}\xi - 2\psi_4\varepsilon_4 + \mu_1 E_1\right),$$

$$\delta = \beta\left(\frac{J-K}{2}\sigma + \Delta\right),$$

and J,K are the Fourier transforms of $J_{qq'}$ and $K_{qq'}$ at $\mathbf{k}=0$.

Equations for polarization and strain are

$$\sigma_4 = c_{44}^{E0}\varepsilon_4 - e_{14}^0 E_1 + 2\frac{\psi_4}{v}\xi,$$
$$P_1 = e_{14}^0\varepsilon_4 + \chi_{11}^{\varepsilon 0}E_1 + \frac{\mu_1}{v}\xi. \tag{2.2}$$

The other calculated static characteristics are the piezomodule

$$d_{14} = \left(\frac{\partial P_1}{\partial\sigma_4}\right)_{E_1} = d_{14}^0 - \frac{s_{44}^{E0}\mu_1'\beta\psi_4}{v}f_2(\xi,\sigma), \tag{2.3}$$

dielectric permittivity of a free crystal

$$\varepsilon_{11}^{\sigma} = 1 + 4\pi\left(\frac{\partial P_1}{\partial E_1}\right)_{\sigma_4} = \varepsilon_{11}^{\sigma 0} + 4\pi\frac{\beta(\mu_1')^2}{2v}f_2(\xi,\sigma), \tag{2.4}$$

compliance

$$s_{44}^{E} = \left(\frac{\partial\varepsilon_4}{\partial\sigma_4}\right)_{E_1} = s_{44}^{E0} + (s_{44}^{E0})^2\frac{2\beta\psi_4^2}{v}f_2(\xi,\sigma), \tag{2.5}$$

and elastic constant at constant field

$$c_{44}^{E} = \left(\frac{\partial\sigma_4}{\partial\varepsilon_4}\right)_{E_1} = c_{44}^{E0} - \frac{2\beta\psi_4^2}{v}f_1(\xi,\sigma). \tag{2.6}$$

The following notations are used:

$$f_1(\xi,\sigma) = \frac{\varphi_3}{\varphi_2}, \quad f_2(\xi,\sigma) = \frac{\varphi_3}{\varphi_2 - \Lambda\varphi_3},$$

$$\lambda_1 = 1 - \xi^2 - \sigma^2, \quad \lambda_2 = 2\xi\sigma,$$

$$\varphi_2 = 1 - \frac{\beta J}{2}\lambda_1 - \beta^2\frac{K^2 - J^2}{16}(\lambda_1^2 - \lambda_2^2),$$

$$\varphi_3 = \lambda_1 + \beta\frac{K-J}{4}(\lambda_1^2 - \lambda_2^2),$$

$$s_{44}^{E0} = \frac{1}{c_{44}^{E0}}, \quad d_{14}^0 = \frac{e_{14}^0}{c_{44}^{E0}}, \quad \varepsilon_{11}^{\sigma 0} = 1 + 4\pi\chi_{11}^{\sigma 0},$$

$$\chi_{11}^{\sigma 0} = \chi_{11}^{\varepsilon 0} + e_{14}^0 d_{14}^0, \quad \mu_1' = \mu_1 - 2\psi_4 d_{14}^0,$$

$$\Lambda = \frac{2\beta\psi_4^2 s_{44}^{E0}}{v}.$$

Values of the model parameters providing the best description of these characteristics are given in Table I.

III. VIBRATIONS OF *X* CUTS OF ROCHELLE SALT

In this section we shall consider vibrations of a thin square plate $l\times l$ of Rochelle salt crystal cut in the (100)

TABLE I. Theory parameters used for Rochelle salt (Ref. 11).

J/k_B	K/k_B	Δ/k_B	ψ_4/k_B	c_{44}^{E0}	d_{14}^0	$\chi_{11}^{\sigma 0}$
	K			dyn/cm^2	esu/dyn	
797.36	1468.83	737.33	−760	12.8×10^{10}	1.9×10^{-8}	0.363

$v=0.5219[1+0.00013(T-190)]\times10^{-21}$ cm^3.
$\mu_1=[2.52+0.0066(297-T)]\times10^{-18}$ esu cm.

plane (X cut) induced by time-dependent electric field $E_1=E_{10}\exp(i\omega_E t)$ or shear stress $\sigma_4=\sigma_{40}\exp(i\omega_\sigma t)$. Those fields give rise to the shear strain ε_4. For the sake of simplicity we shall neglect the diagonal strains ε_i $(i=1,2,3)$, which, in fact, are also created in the ferroelectric phase due to nonzero components of elastic constants tensor c_{i4}.

Dynamics of the pseudospin subsystem will be described within the Glauber approach, where the kinetic equations for the time-dependent averages ξ and σ have the form[11]

$$-\alpha\frac{d}{dt}\xi=\xi-\frac{1}{2}\left[\tanh\frac{1}{2}(\gamma+\delta)+\tanh\frac{1}{2}(\gamma-\delta)\right],$$
$$-\alpha\frac{d}{dt}\sigma=\sigma-\frac{1}{2}\left[\tanh\frac{1}{2}(\gamma+\delta)-\tanh\frac{1}{2}(\gamma-\delta)\right]. \tag{3.1}$$

Here α is the parameter setting the scale of the dynamic processes in the pseudospin subsystem. The best description of microwave permittivity[11] is obtained at $\alpha=1.7\times10^{-13}$ s. It should be noted that Eqs. (3.1) formally are relations of the form

$$\frac{d\zeta}{dt}=A\frac{\partial G}{\partial\zeta}$$

($\zeta=\xi,\sigma$ are the dynamic variables of the system, G is its thermodynamic potential, A is a certain constant). This kinetic equation is usually used for description of the order-parameter dynamics and sound attenuation in ferroelectric crystals,[15,19] with the phenomenological thermodynamic potential G presented as a series expansion in the order parameter. In our case, the model thermodynamic potential (2.2) is used.

Dynamics of the strain ε_4 will be described by the standard method, using classical (Newtonian) equations of motion[13] of an elementary volume

$$\rho\frac{\partial^2\eta_i}{\partial t^2}=\sum_k\frac{\partial\sigma_{ik}}{\partial x_k}, \tag{3.2}$$

where $\rho=1.767$ g/cm^3 is the crystal density, η_i are the displacements of an elementary volume along the axis x_i, and σ_{ik} are components of the mechanical stress tensor. We need to determine the displacements η_2 and η_3, giving the shear strain

$$\varepsilon_4=\frac{\partial\eta_2}{\partial z}+\frac{\partial\eta_3}{\partial y}.$$

Taking into account Eq. (2.2) for $\sigma_{23}=\sigma_4$, as well as the fact that the diagonal strains are assumed equal to zero,

$$\varepsilon_2=\frac{\partial\eta_2}{\partial y}=0,\quad \varepsilon_3=\frac{\partial\eta_3}{\partial z}=0,$$

the expressions (3.2) for $i=2,3$ reduce to two equations,

$$\rho\frac{\partial^2\eta_2}{\partial t^2}=c_{44}^{E0}\frac{\partial^2\eta_2}{\partial z^2}+\frac{2\psi_4}{v}\frac{\partial\xi}{\partial z},$$
$$\rho\frac{\partial^2\eta_3}{\partial t^2}=c_{44}^{E0}\frac{\partial^2\eta_3}{\partial y^2}+\frac{2\psi_4}{v}\frac{\partial\xi}{\partial y}. \tag{3.3}$$

At small deviations from the equilibrium the dynamic variables ξ, σ, and ε_4 can be presented as sums of the equilibrium values and of the fluctuational deviations

$$\xi=\tilde{\xi}+\xi_t,\quad \sigma=\tilde{\sigma}+\sigma_t,\quad \varepsilon_4=\tilde{\varepsilon}_4+\varepsilon_{4t}=\tilde{\varepsilon}_4+\frac{\partial\eta_{2t}}{\partial z}+\frac{\partial\eta_{3t}}{\partial y}.$$

Equations (3.1) and (3.3) can be expanded in terms of these deviations up to the linear terms. For the fluctuation parts we obtain the following system of equations:

$$-\alpha\frac{d}{dt}\xi_t+a_1\xi_t+a_2\sigma_t+a_{01}\left[\frac{\partial\eta_{2t}}{\partial z}+\frac{\partial\eta_{3t}}{\partial y}\right]=a_{02}E_1,$$
$$-\alpha\frac{d}{dt}\sigma_t+b_1\xi_t+b_2\sigma_t+b_{01}\left[\frac{\partial\eta_{2t}}{\partial z}+\frac{\partial\eta_{3t}}{\partial y}\right]=b_{02}E_1,$$
$$\rho\frac{\partial^2\eta_{2t}}{\partial t^2}=c_{44}^{E0}\frac{\partial^2\eta_{2t}}{\partial z^2}+\frac{2\psi_4}{v}\frac{\partial\xi_t}{\partial z}, \tag{3.4}$$
$$\rho\frac{\partial^2\eta_{3t}}{\partial t^2}=c_{44}^{E0}\frac{\partial^2\eta_{3t}}{\partial y^2}+\frac{2\psi_4}{v}\frac{\partial\xi_t}{\partial y},$$

with

$$a_1=-1+\beta\frac{J+K}{4}\lambda_1,\quad a_2=\beta\frac{K-J}{4}\lambda_2,$$
$$a_{01}=-\beta\psi_4\lambda_1,\quad a_{02}=-\frac{\beta\mu_1}{2}\lambda_1,$$
$$b_1=-\beta\frac{J+K}{4}\lambda_2,\quad b_2=-1-\beta\frac{J+K}{4}\lambda_2,$$
$$b_{01}=\beta\psi_4\lambda_2,\quad b_{02}=\frac{\beta\mu_1}{2}\lambda_2.$$

All further consideration will be based on system (3.4).

Solving the first two equations of (3.4) at $\eta_{2t}=\eta_{3t}=0$ (regime of a mechanically clamped crystal), we find

$$\xi_t=\sum_{i=1}^{2}C_i\exp(-t/\tau_i)+F_1(\alpha\omega_E)E_{10}\exp(i\omega_E t),$$

where

$$F_1(\alpha\omega)=\frac{i\alpha\omega\lambda_1+\varphi_3}{(i\alpha\omega)^2+(i\alpha\omega)\varphi_1+\varphi_2},$$

$$F_1(0) = f_1(\xi,\sigma), \quad \varphi_1 = 2 - \frac{\beta J}{2}\lambda_1.$$

The relaxation times are

$$\tau_{1,2}^{-1} = \frac{1}{2\alpha}\left[-\varphi_1 \mp \sqrt{\varphi_1^2 - 4\varphi_2}\right]. \tag{3.5}$$

τ_1 exhibits critical slowing down and τ_2 has only weak peculiarities at the transition points. However, both of these times remain finite at the transition points, which is in accordance with experimental data.[12]

The corresponding dynamic dielectric permittivity of a mechanically clamped crystal is[11]

$$\varepsilon_{11}^{\varepsilon}(\omega) = \varepsilon_{11}^{\varepsilon 0} + 4\pi\frac{\beta\mu_1^2}{2v}F_1(\alpha\omega), \quad \varepsilon_{11}^{\varepsilon 0} = 1 + 4\pi\chi_{11}^{\varepsilon 0}. \tag{3.6}$$

It can be presented as a sum of two Debye terms, where the contribution related to τ_2 is different from zero only in the ferroelectric phase and even then it is several orders smaller than the one related to τ_1 (see Ref. 11 for details).

Hereafter, we shall not impose any artificial conditions for the displacements η_{2t}, η_{3t}. We shall look for solutions of the system (3.4) in the form of harmonic waves

$$\begin{aligned}
\xi_t &= \xi_E(y,z)\exp(i\omega_E t) + \xi_\sigma(y,z)\exp(i\omega_\sigma t),\\
\sigma_t &= \sigma_E(y,z)\exp(i\omega_E t) + \sigma_\sigma(y,z)\exp(i\omega_\sigma t),\\
\varepsilon_{4t} &= \varepsilon_{4E}(y,z)\exp(i\omega_E t) + \varepsilon_{4\sigma}(y,z)\exp(i\omega_\sigma t),\\
\eta_{2t} &= \eta_{2E}(z)\exp(i\omega_E t) + \eta_{2\sigma}(z)\exp(i\omega_\sigma t),\\
\eta_{3t} &= \eta_{3E}(y)\exp(i\omega_E t) + \eta_{3\sigma}(y)\exp(i\omega_\sigma t).
\end{aligned} \tag{3.7}$$

The first two equations of (3.4) give

$$\begin{aligned}
\xi_E(y,z) &= -\beta\psi_4 F_1(\alpha\omega_E)\varepsilon_{4E}(y,z) + \frac{\beta\mu_1}{2}F_1(\alpha\omega_E)E_{10},\\
\xi_\sigma(y,z) &= -\beta\psi_4 F_1(\alpha\omega_\sigma)\varepsilon_{4\sigma}(y,z).
\end{aligned} \tag{3.8}$$

Taking into account (3.7) and (3.8), from the two last equations of (3.4), it follows that

$$\eta_{2E} = \frac{\tilde{c}_{44}^E(\alpha\omega_E)}{\rho(i\omega_E)^2}\frac{\partial^2\eta_{2E}}{\partial z^2}, \quad \eta_{3E} = \frac{\tilde{c}_{44}^E(\alpha\omega_E)}{\rho(i\omega_E)^2}\frac{\partial^2\eta_{3E}}{\partial y^2},$$

$$\eta_{2\sigma} = \frac{\tilde{c}_{44}^E(\alpha\omega_\sigma)}{\rho(i\omega_\sigma)^2}\frac{\partial^2\eta_{2\sigma}}{\partial z^2}, \quad \eta_{3\sigma} = \frac{\tilde{c}_{44}^E(\alpha\omega_\sigma)}{\rho(i\omega_\sigma)^2}\frac{\partial^2\eta_{3\sigma}}{\partial y^2},$$

where

$$\tilde{c}_{44}^E(\alpha\omega) = c_{44}^{E0} - \frac{2\beta\psi_4^2}{v}F_1(\alpha\omega).$$

Assuming the plane-wave form of η_{iE},

$$\eta_{2E} \sim \exp(ik_E z), \quad \eta_{3E} \sim \exp(ik_E y),$$

and similarly for $\eta_{2\sigma}$, $\eta_{3\sigma}$, we find the dispersion law for the vibrations

$$k_E = \frac{\sqrt{\rho}\omega_E}{\sqrt{\tilde{c}_{44}^E(\alpha\omega_E)}}, \quad k_\sigma = \frac{\sqrt{\rho}\omega_\sigma}{\sqrt{\tilde{c}_{44}^E(\alpha\omega_\sigma)}}. \tag{3.9}$$

The boundary conditions are set as follows:

$$\varepsilon_{4E}(0,0) = \varepsilon_{4E}(0,l) = \varepsilon_{4E}(l,0) = \varepsilon_{4E}(l,l) = \varepsilon_{0E},$$

$$\varepsilon_{4\sigma}(0,0) = \varepsilon_{4\sigma}(0,l) = \varepsilon_{4\sigma}(l,0) = \varepsilon_{4\sigma}(l,l) = \varepsilon_{0\sigma}.$$

The values of ε_{0E} and $\varepsilon_{0\sigma}$ are determined from (2.2), using relations (3.8) between ε_{4E} and ξ_E, and between $\varepsilon_{4\sigma}$ and ξ_σ,

$$\varepsilon_{0E} = \frac{d_{14}^0 - \dfrac{\beta\mu_1\psi_4 s_{44}^{E0}}{v}F_1(\alpha\omega_E)}{1 - \Lambda F_1(\alpha\omega_E)}E_{10},$$

$$\varepsilon_{0\sigma} = \frac{s_{44}^{E0}}{1 - \Lambda F_1(\alpha\omega_E)}\sigma_{40}.$$

With these boundary conditions we find that

$$\varepsilon_{4E}(y,z) = \frac{\varepsilon_{0E}}{2}\left[\cos k_E z + \cos k_E y - \tan\frac{k_E l}{2}(\sin k_E y + \sin k_E z)\right],$$

and similarly for $\varepsilon_{4\sigma}(y,z)$.

Using Eqs. (2.2) and (3.8), we can find polarization

$$P_1(y,z,t) = P_{1E}(y,z)\exp(i\omega_E t) + P_{1\sigma}(y,z)\exp(i\omega_\sigma t),$$

where

$$\begin{aligned}
P_{1E}(y,z) &= \left[e_{14}^0 - \frac{\beta\mu_1\psi_4}{v}F_1(\alpha\omega_E)\right]\varepsilon_{4E}(y,z)\\
&\quad + \left[\chi_{11}^{\varepsilon 0} + \frac{\beta\mu_1^2}{2v}F_1(\alpha\omega_E)\right]E_{10},\\
P_{1\sigma}(y,z) &= \left[e_{14}^0 - \frac{\beta\mu_1\psi_4}{v}F_1(\alpha\omega_\sigma)\right]\varepsilon_{4\sigma}(y,z).
\end{aligned}$$

Observable dynamic characteristics of the system: dielectric susceptibility at constant stress $\chi_{11}^{\sigma}(\omega_E)$, piezomodule $d_{14}(\omega_\sigma)$, and elastic compliance at constant field $s_{44}^E(\omega_\sigma)$, are expressed as appropriate derivatives from the integrals over the sample volume of polarization or strain

$$\chi_{11}^{\sigma}(\omega_E) = \frac{1}{l^2}\frac{\partial}{\partial E_{10}}\int_0^l dy\int_0^l dz P_{1E}(y,z),$$

$$d_{14}(\omega_\sigma) = \frac{1}{l^2}\frac{\partial}{\partial \sigma_{40}}\int_0^l dy\int_0^l dz P_{1\sigma}(y,z),$$

$$s_{44}^{E}(\omega_\sigma)=\frac{1}{l^2}\frac{\partial}{\partial\sigma_{40}}\int_0^l dy\int_0^l dz\varepsilon_{4\sigma}(y,z).$$

Thus

$$\begin{aligned}\varepsilon_{11}^{\sigma}(\omega)&=1+4\pi\chi_{11}^{\sigma}(\omega),\\ \chi_{11}^{\sigma}(\omega)&=\frac{R(\omega)-1}{R(\omega)}\left[\chi_{11}^{\varepsilon 0}+\frac{\beta\mu_1^2}{2v}F_1(\alpha\omega)\right]\\ &\quad+\frac{1}{R(\omega)}\left[\chi_{11}^{\sigma 0}+\frac{\beta(\mu_1')^2}{2v}F_2(\alpha\omega)\right],\end{aligned}\tag{3.10}$$

$$s_{44}^{E}(\omega)=\frac{1}{R(\omega)}\left\{s_{44}^{E0}+(s_{44}^{E0})^2\frac{2\beta\psi_4^2}{v}F_2(\alpha\omega)\right\},\tag{3.11}$$

$$d_{14}(\omega)=\frac{1}{R(\omega)}\left\{d_{14}^{0}-\frac{s_{44}^{E0}\mu_1'\beta\psi_4}{v}F_2(\alpha\omega)\right\},\tag{3.12}$$

where

$$F_2(\omega)=\frac{i\alpha\omega\lambda_1+\varphi_3}{(i\alpha\omega)^2+i\alpha\omega[\varphi_1-\Lambda\lambda_1]+[\varphi_2-\Lambda\varphi_3]},$$

$$F_2(0)=f_2(\xi,\sigma),$$

$$\frac{1}{R(\omega)}=\frac{2}{kl}\tan\frac{kl}{2}.$$

Let us analyze the above results. In the static limit [$\omega\to 0$, $R(\omega)\to 1$] from (3.10) we obtain the static permittivity of a free crystal (2.4); in the high-frequency limit [$R(\omega)\to\infty$] we get a dynamic permittivity (3.6) of a mechanically clamped crystal, exhibiting relaxational dispersion in the microwave region. Thus, Eq. (3.10) explicitly describes the effect of crystal clamping by high-frequency electric field. Elastic compliance $s_{44}^{E}(\omega)$ and piezomodule $d_{14}(\omega)$ in the high-frequency limit turn to zero, which is also a manifestation of the clamping effect. At $\omega\to 0$ Eqs. (3.11) and (3.12) transform into s_{44}^{E} (2.5) and d_{14} (2.3).

In the intermediate frequency region, the calculated characteristics have a resonance dispersion with numerous peaks at frequencies where $\mathrm{Re}[R(\omega_n)]=0$ or $\mathrm{Re}[k_n l/2]=\pi(2n+1)/2$. Frequency variation of $\tilde{c}_{44}^{E}(\omega)$ is perceptible only in the region of the microwave dispersion of the dielectric susceptibility. Below this region $\tilde{c}_{44}^{E}(\omega)$ is practically frequency independent and coincides with the static elastic constant c_{44}^{E}. Since the resonance frequencies are expected to be in the 10^4-10^7 Hz range, depending on temperature and sample dimensions, we can neglect the frequency dependence of $\tilde{c}_{44}^{E}(\omega)$ and reduce an equation for the resonance frequencies to

$$\omega_n=\frac{\pi(2n+1)}{l}\sqrt{\frac{c_{44}^{E}}{\rho}}.\tag{3.13}$$

Resonance frequencies are inversely proportional to sample dimensions. Universal (sample independent) is the frequency constant $2\pi\omega_0 l$.

IV. SOUND PROPAGATION IN ROCHELLE SALT (90° *Z* CUTS)

Pulsed ultrasonics provide a powerful and convenient tool for the investigation of mechanical and piezoelectric properties of crystals. The ultrasound wavelength is usually much smaller than the sample dimensions. Therefore the dynamical variables (displacements, order parameter, etc.) depend only on the spatial coordinate which is the direction of sound propagation.

Within the presented above approach one can readily calculate the characteristics of ultrasound propagation in Rochelle salt. From the point of view of the developed model, one should consider the transverse sound wave, which propagates in the so-called 90° *Z* cuts of Rochelle salt (thin bars cut along [001]) and is polarized along [010]. Among $\partial\eta_i/\partial x_j$ the only nonzero derivative is $\partial\eta_2/\partial z$; therefore, instead of (3.4) we have

$$\begin{aligned}&-\alpha\frac{d}{dt}\xi_t+a_1\xi_t+a_2\sigma_t+a_{01}\varepsilon_{4t}=0,\\ &-\alpha\frac{d}{dt}\sigma_t+b_1\xi_t+b_2\sigma_t+b_{01}\varepsilon_{4t}=0,\\ &\rho\frac{\partial^2\eta_{2t}}{\partial t^2}=c_{44}^{E0}\frac{\partial^2\eta_{2t}}{\partial z^2}+\frac{2\psi_4}{v}\frac{\partial\xi_t}{\partial z}.\end{aligned}\tag{4.1}$$

One can easily verify that for the system (4.1) the frequency dependence of the wave vector

$$k_\sigma=\frac{\sqrt{\rho}\omega_\sigma}{\sqrt{\tilde{c}_{44}^{E}(\alpha\omega_\sigma)}}$$

coincides with that obtained in the previous section dispersion law of (100) plate vibrations (3.9).

This expression gives the ultrasound velocity $V=\omega/\mathrm{Re}[k]$ and the contribution of the ordering subsystem into ultrasound attenuation for a 90° *Z* cut of Rochelle salt $\varkappa_t=-\mathrm{Im}[k]$. Background contributions into observed attenuation (inherent to pulsed method: beam spreading, pulse distortion, etc.) will be described by a constant frequency and temperature-independent term $\varkappa_0$, such that

$$V(\omega)=\mathrm{Re}\sqrt{\frac{\tilde{c}_{44}^{E}(\alpha\omega)}{\rho}},\tag{4.2}$$

$$\varkappa(\omega)=\varkappa_0-\mathrm{Im}\left[\frac{\sqrt{\rho}\omega}{\sqrt{\tilde{c}_{44}^{E}(\alpha\omega)}}\right].\tag{4.3}$$

At low frequencies, when $\omega\tau_1\ll 1$ and $\mathrm{Re}[\tilde{c}_{44}^{E}(\alpha\omega)]\gg\mathrm{Im}[\tilde{c}_{44}^{E}(\alpha\omega)]$ (up to about $\sim$100 MHz, maybe except the vicinity of the transition point), in a quadratic with respect to $\omega\tau_1$ approximation we have

$$\tilde{c}_{44}^{E}(\alpha\omega)\simeq c_{44}^{E0}+(c_{44}^{E}-c_{44}^{E0})\frac{1+i\omega\tau_1}{1+\omega^2\tau_1^2}$$

(the Debye contribution related to the relaxation time τ_2 is neglected). Thence we obtain the approximate formulas for

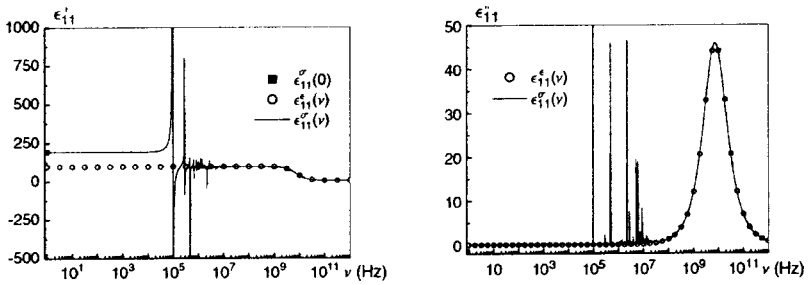

FIG. 1. Frequency dependence of dielectric permittivity of Rochelle salt at 289 K. Solid line: Eq. (3.10). ○: Dynamic permittivity of a clamped crystal (3.6). ■: Static permittivity of a free crystal. Lines and symbols: A theory.

low-frequency sound velocity and attenuation

$$V^2 = V_0^2 + \frac{1}{\rho}\frac{c_{44}^E - c_{44}^{E0}}{1+\omega^2\tau_1^2}, \quad \varkappa(\omega) = \varkappa_0 + \frac{V_0^2 - V^2}{2V^3}\omega^2\tau_1,$$

$$V_0^2 = \frac{c_{44}^{E0}}{\rho}.$$

In this approximation the sound velocity is hardly frequency dependent, whereas attenuation is proportional to the square of frequency.

V. NUMERICAL ANALYSIS

No additional theory parameters should be determined apart from those found in Ref. 11 and given in Table I. We have, however, to specify the sample dimensions, which determine the positions of the resonance peaks.

A. Dynamic response of Rochelle salt

First let us consider the calculated dielectric susceptibility, piezomodule, and elastic compliance of an *X* cut of Rochelle salt. A square plate with dimensions 1×1 cm^2 is assumed.

Figure 1 shows the frequency dependence of dynamic permittivity of Rochelle salt in the ferroelectric phase. The obtained evolution of the permittivity is analogous to the experimental one,[1] except for the domain-related dispersion below 1 kHz. Similar behavior is observed also in the paraelectric phases. At $\omega\to0$ the static permittivity of a free crystal is obtained; in the region $10^5\div10^7$ Hz a resonance dispersion is observed. Magnitudes of the resonance peaks decrease upon increase of frequency. Above the resonances crystals get clamped by a high-frequency field, and the permittivity of a clamped crystal exhibits a relaxational dispersion in the microwave region.

The piezomodule $d_{14}(\omega)$, the frequency dependence of which is depicted in Fig. 2, as well as the elastic compliance $s_{44}^E(\omega)$, show a resonance dispersion in the $10^5\div10^7$ Hz region, turn to zero above the resonances and to their static values below them.

Figures 3 and 4 illustrate the temperature dependences of dynamic permittivity at different frequencies. The temperature curves of the dynamic piezomodule and compliance are similar. Below the frequency of the first resonance peak, the temperature variation of dynamic permittivity essentially coincides with that of the static permittivity of a free crystal. Near the resonance frequencies, the sharp peaks in the temperature curve of permittivity appear, the number of which increases with increase of frequency, whereas the magnitudes decrease. Upon further increase of frequency, numerous resonance peaks of small amplitude arise around the curve of clamped permittivity. At even higher frequencies the peaks disappear, and the typical smooth curve of the clamped permittivity is observed.

B. Sound attenuation

In Fig. 5 we show the temperature dependence of ultrasound attenuation for the transverse wave propagating in the 90° *Z* cut of Rochelle salt. Near the Curie points a sharp increase of attenuation is obtained, in accordance with the Landau and Khalatnikov theory.[18] A qualitative agreement with experiment is obtained. The experimental attenuation in the ferroelectric phase strongly exceeds the theoretical one; this should be attributed to domain effects.

A certain quantitative discrepancy between theory and experiment takes place in the paraelectric phases as well. The theoretical values are usually smaller than the experimental ones. This should be explained by the existence of additional sound absorption mechanisms which are not taken into account by the proposed model. Another factor is the possible nonlinearity that could occur during the experimental mea-

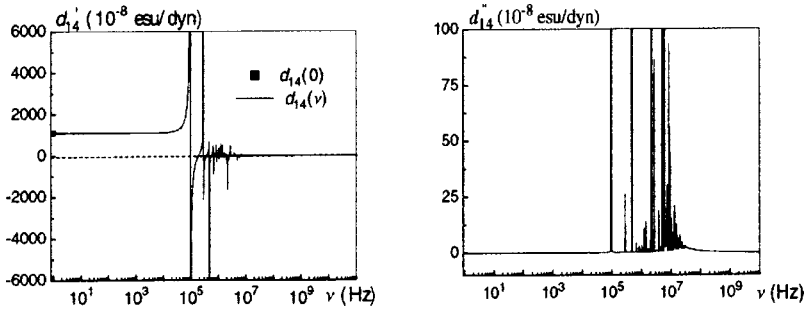

FIG. 2. Frequency dependence of the dynamic piezomodule of Rochelle salt at 289 K. ■: Static piezomodule (2.3). Lines and symbols: A theory.

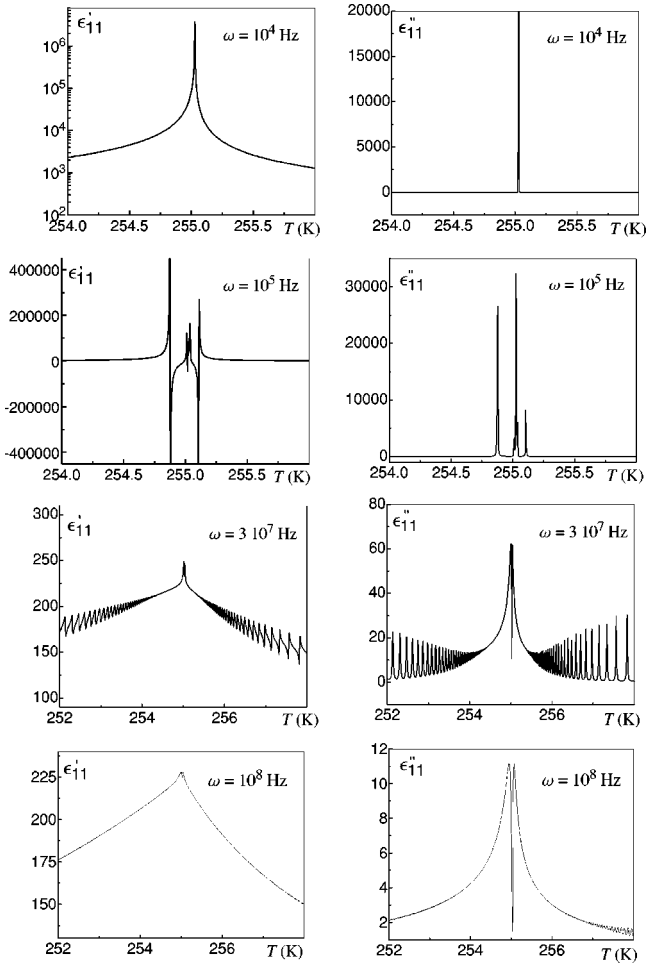

FIG. 3. Temperature dependences of dynamic dielectric permittivity of Rochelle salt (3.10) near the lower transition point at different frequencies.

surements, increasing thus the measured value of attenuation (due to generation of higher harmonics).

In the low-frequency range ($\omega \lesssim 10^6$ Hz), as expected, attenuation varies proportionally to the square of frequency. The closer the temperature is to the Curie point, the larger is the rate of this variation (Fig. 6).

An interesting effect is observed at high frequencies. Somewhat below the region of the microwave dispersion of dielectric permittivity, the theory predicts a sharp increase of attenuation with increase of frequency; after that the saturation is observed (Fig. 6). Such high values of attenuation at saturation, in fact, mean absence of sound propagation (cutoff frequency). One may notice that the position of the cutoff frequency is in the region of a fast increase in the imaginary part of the dielectric permittivity (Fig. 6). In the paraelectric phases the cutoff frequency decreases with approaching the transition point (Fig. 7). Experimental measurements of sound attenuation in Rochelle salt so far have been restricted to the MHz region. The extension of sound attenuation measurements to higher frequencies (possibly up to the microwave region) is thus of great interest.

At the frequency of the microwave dispersion of permittivity, a sharp increase of sound velocity should be observed

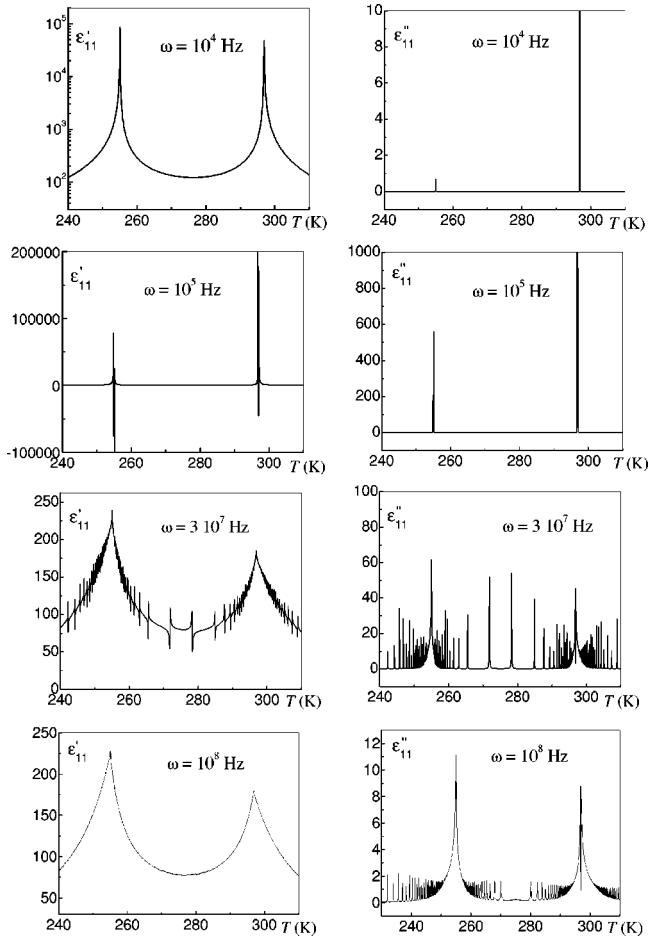

FIG. 4. Same in a wide temperature range.

(see Fig. 7), after which the frequency curve of velocity $V(\nu)$ saturates. The saturation value is temperature independent and equal to $V_0 = \sqrt{c_{44}^{E0}/\rho}$.

VI. CONCLUSIONS

In this paper we have applied the previously proposed modification of the two-sublattice Mitsui model with piezoeffect to description of a dynamic response of Rochelle salt in the entire frequency range from the static limit (1 kHz in

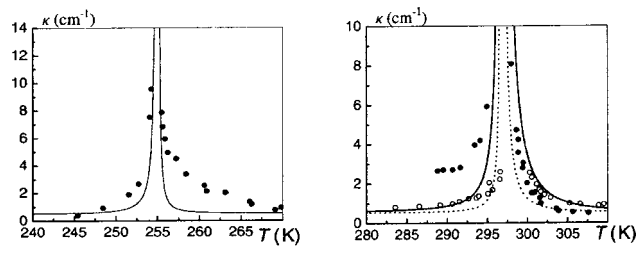

FIG. 5. Temperature dependence of attenuation for the transverse wave propagating in the 90° Z cut of Rochelle salt near the Curie points at $\nu = 5 \times 10^6$ Hz (solid lines, ●, Refs. 14 and 15) and $\nu = 10^7$ Hz, (dashed line, ○, Ref. 16). Lines: Eq. (4.3) with $\kappa_0 = 0.5$ cm^{-1}.

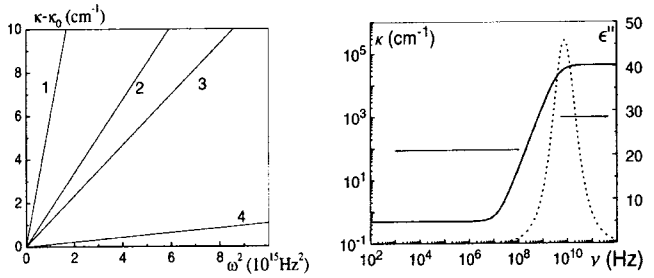

FIG. 6. Frequency dependence of attenuation at different temperatures (K). Left: (1) 298, (2) 299, (3) 300, (4) 305. Right: 289 (solid lines). Dashed line: Imaginary part of dielectric permittivity.

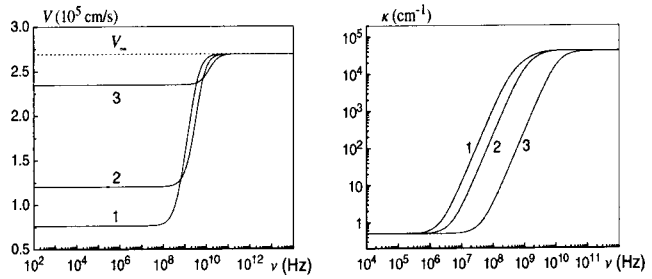

FIG. 7. Frequency dependences of sound velocity and attenuation at different temperatures (K): (1) 298, (2) 300, (3) 350.

the ferroelectric phase) up to the THz region. Dynamic dielectric, piezoelectric, and elastic characteristics are calculated. Experimentally observed evolution of dynamic permittivity from the static free crystal value via the piezoelectric resonances to the clamped crystal value and to the microwave relaxation is obtained. Within the same approach the sound velocity and attenuation for a transverse wave propagating in the 90° *Z* cut are calculated. A qualitative agreement with experiment for sound attenuation is obtained. To reach a satisfactory quantitative description of some of the experimental data, one should take into account nonlinear processes and/or additional mechanisms of sound attenuation not included in the present model. This is the subject of our further studies. An existence of a cutoff frequency for sound propagation is expected, which frequency position correlates with the start of a fast increase in the imaginary part of the dielectric permittivity. Experimental measurements of sound attenuation in Rochelle salt in this frequency range have not been performed and are of great interest.

ACKNOWLEDGMENT

The authors acknowledge support from the State Foundation for Fundamental Studies of Ukraine, Project No. 02.07/00310.

[1] Y. M. Poplavko, V. V. Meriakri, P. Pereverzeva, V. V. Alesheckin, and V. I. Molchanov, Fiz. Tverd. Tela (Leningrad) **15**, 2515 (1974) [Sov. Phys. Solid State **15**, 1672 (1974)].
[2] A. V. Shyl'nikov, N. M. Galijarova, E. G. Nadolinskaya, S. V. Gorin, and M. A. Shuvaev, Kristallografiya **31**, 326 (1986) [Sov. Phys. Crystallogr. **31**, 192 (1986)].
[3] J. F. Araujo, J. Mendes Filho, F. E. A. Melo, F. V. Letelier, and A. S. Chaves, Phys. Rev. B **57**, 783 (1998).
[4] H. Mueller, Phys. Rev. **58**, 565 (1940).
[5] T. Mitsui, Phys. Rev. **111**, 1259 (1958).
[6] R. J. Glauber, J. Math. Phys. **4**, 294 (1963).
[7] R. R. Levitskii, I. R. Zachek, and V. I. Varanitskii, Ukr. J. Phys. **25**, 1766 (1980) (in Russian).
[8] B. Zeks, G. C. Shukla, and R. Blinc, J. Phys. (Paris), Colloq. **33**, C2-67 (1972).
[9] R. Blinc and B. Žekš, *Soft Modes in Ferroelectrics and Antiferroelectrics* (Elsevier, New York, 1974).
[10] R. R. Levitskii, I. R. Zachek, T. M. Verkholyak, and A. P. Moina, Condens. Matter Phys. **6**, 261 (2003).
[11] R. R. Levitskii, I. R. Zachek, T. M. Verkholyak, and A. P. Moina, Phys. Rev. B **67**, 174112 (2003).
[12] F. Sandy and R. V. Jones, Phys. Rev. **168**, 481 (1968).
[13] W. P. Mason, *Piezoelectric Crystals and Their Application to Ultrasonics* (Van Nostrand, New York, 1950).
[14] O. A. Shustin, T. S. Velichkina, K. N. Baranskii, and I. A. Iakovlev, Zh. Eksp. Teor. Fiz. **40**, 979 (1961) [Sov. Phys. JETP **13**, 683 (1961)].
[15] I. A. Iakovlev and T. S. Velichkina, Usp. Fiz. Nauk **63**, 411 (1957)
[16] W. J. Price, Phys. Rev. **75**, 946 (1949).
[17] R. Kawashima and I. Tatsuzaki, J. Phys. Soc. Jpn. **42**, 564 (1977).
[18] L. D. Landau and I. M. Khalatnikov, Dokl. Akad. Nauk SSSR **96**, 469 (1954).
[19] D. G. Sannikov, Fiz. Tverd. Tela (Leningrad) **4**, 1619 (1962) [Sov. Phys. Solid State **4**, 1187 (1962)].